

Sub-10 nm nanopantography

Siyuan Tian,^{1,a)} Vincent M. Donnelly,^{1,b)} Paul Ruchhoeft,^{2,c)} and Demetre J. Economou^{1,b)}

¹*Plasma Processing Laboratory, Department of Chemical and Biomolecular Engineering,
University of Houston, Houston, Texas 77204, USA*

²*Department of Electrical and Computer Engineering, University of Houston, Houston, Texas 77204, USA*

(Received 28 September 2015; accepted 30 October 2015; published online 13 November 2015)

Nanopantography, a massively parallel nanopatterning method over large areas, was previously shown to be capable of printing 10 nm features in silicon, using an array of 1000 nm-diameter electrostatic lenses, fabricated on the substrate, to focus beamlets of a broad area ion beam on selected regions of the substrate. In the present study, using lens dimensional scaling optimized by computer simulation, and reduction in the ion beam image size and energy dispersion, the resolution of nanopantography was dramatically improved, allowing features as small as 3 nm to be etched into Si.

© 2015 AIP Publishing LLC. [<http://dx.doi.org/10.1063/1.4935552>]

Lithography at the sub-10 nm scale is essential for the fabrication of future integrated circuits, as well as many other nanodevices. For example, quantum and single electron devices require a critical dimension (e.g., dot, wire, or ribbon) less than 10 nm to enhance quantum effects, leading to greatly improved or totally new device characteristics.^{1–3} Plasmonic nanodevices, which overcome the diffraction limit and display extreme enhancement of electromagnetic energy in subwavelength features due to collective excitation of conduction electrons, have great potential in applications including nanophotonics, biosensors, chemical sensors, and photovoltaic cells.^{4–6} Sensors, which can detect and rapidly identify macromolecules, including DNA sequencing, by changes in current or other signals as they pass through holes require the formation of <5 nm-diameter nanopores in ultra-thin films.^{7–12} In addition, graphene and other 2-D materials have recently been synthesized in large sheets, and a large area method for creating nanopatterns in such films offers an opportunity for fabrication of the next generation electronic and photonic devices.^{13–19} Advances in these technologies demand a method to fabricate nanopatterns over large areas, with high throughput and low cost. Photolithography can define such small dimensions by implementing multiple patterning and extreme ultraviolet (EUV) light sources, but it is so complex and expensive that is only suited for large-volume applications. Less complex tools either suffer from resolution or throughput problems, so there is a clear need for developing lower complexity lithography under the 10 nm scale. A scanning electron beam is capable of writing ~2 nm features, but not in a parallel manner.²⁰ Very small features can also be formed by self-assembly,^{21–24} but the types of patterns that can be formed are limited. Scanning probes can manipulate single atoms,^{25–27} but not in a massively parallel manner. Nanoimprint lithography (NIL) is a promising method for high throughput and low cost fabrication; however, at the sub-10 nm scale, a few lingering

barriers such as defects, template patterning, and wear must be overcome to enable large scale implementation.

Nanopantography is a method for massively parallel writing of nanopatterns over large areas. Billions of electrostatic lenses are first fabricated on top of a wafer using conventional semiconductor manufacturing processes. A broad area, collimated, monoenergetic ion beam is then directed towards the wafer surface. By applying an appropriate DC voltage to the lens array with respect to the wafer, the ion beamlet entering each lens converges to a fine spot focused on the wafer surface that can be 100 times smaller than the diameter of the lens. By controlling the tilt of the substrate with respect to the ion beam, the focused ion beamlets can “write” a desired pattern in a massively parallel fashion in selected areas of the substrate. Previously, nanopantography was used to etch ~10 nm-diam. holes in Si, by simultaneous exposure to a monoenergetic Ar⁺ ion beam and Cl₂ gas,²⁸ as well as to deposit 10 nm-diam. Ni dots using a Ni ion beam. Etching of complex patterns was also demonstrated.²⁹ Furthermore, to improve throughput, a two-step process was developed.³⁰ In the first step, short exposure time to nanopantographic etching was used to break through the native oxide of Si, creating an ultrathin (~2 nm) mask on the wafer surface. In the second step, the patterned Si wafer was etched in a chlorine plasma, under photo-assisted etching conditions, using the native oxide as a mask. Under these conditions, it was possible to maintain a moderate etching rate of Si (10 s of nm/min) to fabricate high aspect ratio (>5:1) features into the Si substrate. This was accomplished due to the lack of ions with energies above the threshold for ion-assisted etching, resulting in extremely high selectivity of Si over the SiO₂ mask.

In this letter, a combination of experiments and simulations was used to achieve resolution in the sub-10 nm regime, allowing the creation of patterns with features as small as 3 nm. These appear to be the smallest features ever formed in selected locations in a massively parallel, direct writing process.

Electrostatic lenses were fabricated on Si substrates using standard semiconductor manufacturing techniques. Two sizes of electrostatic lenses were used for most

^{a)}Current address: Lam Research, Fremont, California 94538, USA.
Electronic mail: siyuan.tian@lamresearch.com

^{b)}Electronic addresses: vmdonnelly@uh.edu and economou@uh.edu

^{c)}E-mail: pruchhoeft@uh.edu

experiments. Lens A (Fig. 1) was the same as that described by Tian *et al.*³⁰ This lens had a diameter of $d_l = 650$ nm, a focal length of 1150 nm, and consisted of a 150 nm sputter-deposited Al layer on top of 1000 nm thermally grown oxide on p-type silicon. Lens B had nominal diameter of $d_l = 200$ nm (actual value ranging from 170 nm to 270 nm), a focal length of 330 nm, and consisted of a 30 nm sputter-deposited tungsten layer on top of 300 nm thermally grown oxide on p-type silicon. By applying a DC bias between the metal electrode and the substrate (depicted in Fig. 1), a static electric field was established locally within and around each lens. Ions with kinetic energy E_i flying towards the lens were deflected by the spatially varying field and, under the proper bias voltage ($V_{bias} < E_i$), came to a focus at the bottom of the hole (i.e., on the substrate surface, see Fig. 1). Thinner SiO_2 made it possible to keep the lens aspect ratio unchanged (same lens numerical aperture) while reducing the lens diameter, allowing lens B to produce smaller features. An ion energy of $E_i = 100$ eV was chosen to balance the competing requirements between patterning speed (proportional to $(E_i^{1/2} - E_{th}^{1/2})$, where E_{th} is a threshold energy), and resolution (higher ion energy requires thicker dielectric to avoid breakdown; thicker dielectric results in lower resolution). The breakdown field for thermally grown (dry) oxide can reach 10 MV/cm.^{31–33} This implies that an applied voltage of 100 V requires an oxide thickness of at least 100 nm to minimize the probability of breakdown. Thus, the SiO_2 film could be thinned down to 300 nm, and still have a very low probability of electrical breakdown.

The patterning procedure was similar to that reported previously.²⁸ Samples were first loaded into the processing chamber and positioned perpendicular to the direction of the ion beam. The Si substrate was electrically connected to system ground, while the metal layer on top was biased with a DC voltage which was varied between 80.0 and 98.5 V. A metal grid with 39 μm wide holes was positioned 10 mm above the substrate and grounded. This prevented deflection of the ion beam near the edges of the sample.²⁹ Cl_2 was admitted into the processing chamber yielding a partial pressure of $3.0\text{--}4.0 \times 10^{-5}$ Torr. Ion bombardment promoted surface reactions of adsorbed chlorine with silicon atoms

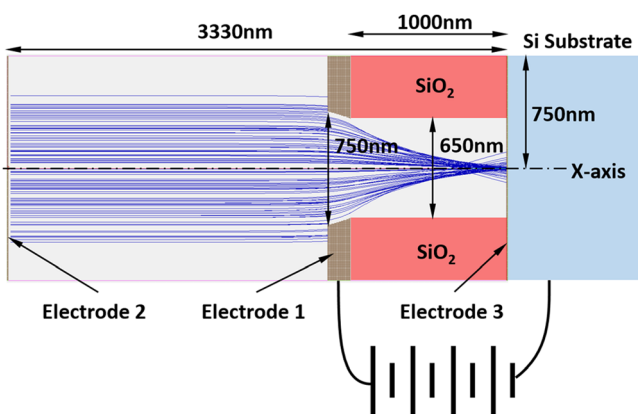


FIG. 1. Geometry of Lens A with the computational domain and sample ion trajectories at a non-optimum focusing voltage. Particle spatial coordinates are recorded when a particle strikes the bottom of the feature (i.e., Si wafer, Electrode 3). Electrode 1 = 95 V, Electrode 2 = 0 V, and Electrode 3 = 0 V.

resulting in ion-assisted etching of silicon at each beamlet focal point.

In nanopantography, an array of lenses simultaneously projects the image of an object (ion source) onto the substrate. For simple, ideal optics

$$\frac{1}{f} = \frac{1}{s_1} + \frac{1}{s_2}, \quad (1)$$

where s_1 and s_2 are the distances from the lens to the object and the image planes, respectively, and f is the focal length. Because the distance to the image is so much smaller than the distance to the object ($s_2 \ll s_1$), $f = s_2$. The lens magnification is

$$M = \frac{s_2}{s_1}. \quad (2)$$

To improve resolution, compared to the previous nanopantography experiments,²⁸ down to an unprecedented size of 3 nm, a smaller ion beam delimiter was used (hole diameter 5 mm), and the distance between the ion source and the sample (s_1) was increased to 60 cm. The first action reduced the object size while the second changed the magnification, both at the cost of a reduced beam flux at the sample surface. To compensate for the reduction in ion flux, the inductively coupled plasma source generating the ion beam was equipped with a pair of co-axial electro-magnets, which, combined with source optimization, resulted in an increase of the plasma density (and ion flux) by one order of magnitude. Under these conditions, a typical ion flux at the sample location was $\sim 1 \mu\text{A}/\text{cm}^2$ before focusing.

Given $f = s_2 = 300$ nm (lens B) and $s_1 = 0.6$ m, the magnification was $M = 5 \times 10^{-7}$. Thus, the diameter of the image (d_i) of the $d_s = 5$ mm diam. ion beam delimiter should be $d_i = M d_s$ or 2.5 nm. The smallest feature we were able to form was ~ 3 nm, close to the theoretical value. A feature size slightly larger than predicted is not surprising, since Eq. (1) assumes paraxial rays and does not account for aberrations. Computer simulation (using SIMION³⁴) were therefore conducted to compare with experimental data and to gain further insight in the behavior of the system under non-ideal conditions. The geometry of the simulation is shown in Fig. 1. The computational domain was 2D-axisymmetric with radius and length equal to 750 and 3330 nm, respectively.

The lens diameter was 650 nm, the metal electrode thickness was 150 nm, and the oxide thickness was 1000 nm as measured from scanning electron micrograph (SEM) images. Due to non-ideal etching of aluminum (Electrode 1) during lens fabrication, the aluminum sidewall was tapered, increasing the diameter at the lens entrance to ~ 750 nm. The electrode voltages were specified, the ion energy distribution (IED) was measured *in situ*, and the ion angular distribution (IAD) was estimated (see below). IED and IAD information was needed to select the initial velocity vector of particles at the launch plane (Electrode 2 in Fig. 1). A particle's coordinates were recorded when the particle struck electrode 3 and plotted as a histogram for 3000 particle flights (Fig. 2). Since the IED was nearly monoenergetic for all ions entering the lenses, and the angular spread of ions at the focus on the surface, determined predominantly by the bending of ions

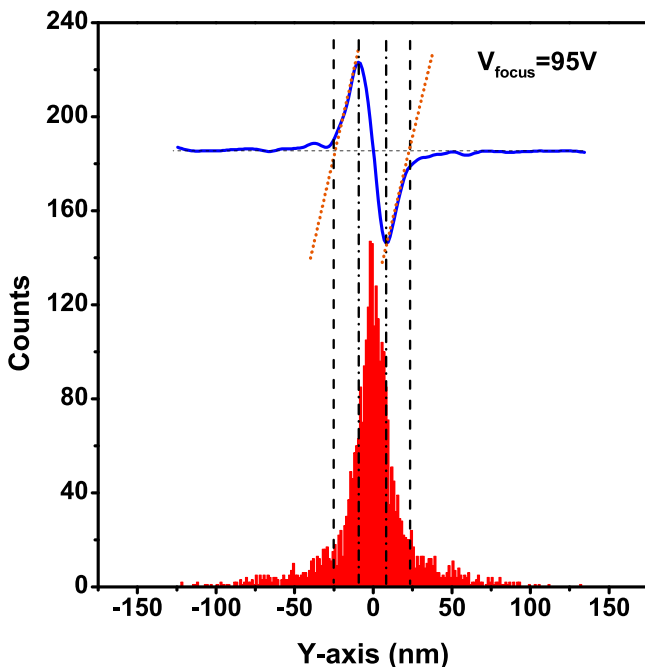


FIG. 2. Histogram of particle landing position at the bottom surface (on the substrate) of Lens A and its first derivative (blue line) for a focusing voltage of 95 V.

entering the lenses near the walls, is $<\pm \arctan(d_l/2f)$ ($<\pm 16^\circ$ for both lenses), we can assume that the Ar^+ ion-assisted etching yield for Si at a given Cl_2 partial pressure in the processing chamber was the same for all ions. Thus, the particle distribution profile on the surface of Electrode 3 (Si substrate) should etch a hole into Si that is the inverse of the profile of Fig. 2.

Since the histogram of particle landing positions is not Gaussian, the usual definition of the full width at half maximum (FWHM) may not be an appropriate measure of the width of the distribution. Instead, the width was defined as the spacing between the minimum and maximum in the first derivative of the histogram (blue curve in Fig. 2), denoted by the vertical dashed-dotted lines. For comparison with measurements of the hole diameters determined from top-down SEM images, a more conservative estimate of the diameter of the feature was determined from the width between the zero crossings of a linear extrapolation of the first derivative of the histogram (vertical dashed lines in Fig. 2).

A nearly monoenergetic Ar^+ ion beam was generated by the 13.56 MHz RF inductively coupled plasma source that operated in pulsed plasma mode, with a peak power of 800 W, a pulsing frequency of 10 kHz, and a duty cycle of 20%. A synchronized DC bias was applied on a boundary electrode in the afterglow (power off) of the pulsed plasma. The bias voltage raised the plasma potential causing positive ions to be expelled from the plasma through a grounded extraction grid.³⁵ The IED was measured *in situ* using a retarding field ion energy analyzer. A Gaussian was fitted to the IED peak, yielding an average ion energy of 107 eV and a FWHM of 4 eV. Under these conditions, the ion beam current density at the sample location was $\sim 0.85 \mu\text{A}/\text{cm}^2$. The ion launch half angle was estimated to be $\sim 0.24^\circ$, calculated from the 2.5 mm radius beam-delimiter aperture and the 600 mm beam drift distance.

Lens A was used to experimentally study the relationship between focusing voltage and etched hole size at the focal point for a given lens diameter. The etched hole size was measured from SEM images with a $\pm 5\%$ error. This error is based on the uncertainty of measuring a perceptible change in image contrast, combined with the size of the scale bar embedded in the SEM image. For lens A, with a diameter of 650 nm, the optimum focusing voltage to form the smallest beam waist on the Si surface was found in experiments and simulations to be 96.8 V. Increasing or decreasing the voltage by 1 V roughly doubled the beam focus diameter at the surface.

Using lens B, the focusing voltage was fixed at the optimum value found experimentally for lens A and the lens diameter was varied. To improve efficiency and reproducibility, lenses were fabricated with different diameters on the same sample. Other key parameters affecting focus (lens height, IED, and IAD) were kept unchanged. Results for two samples, made using identical fabrication procedure, are plotted in Fig. 3. The beam must be focused properly at the base of the lens to achieve the smallest feature size. This minimum size is determined by the magnification and the spherical and chromatic aberrations of the lens. The optimum lens diameter that gives the finest patterned trench width is ~ 185 nm for a fixed lens height of 330 nm. For smaller lens diameters, the (constant) focusing voltage is too far from the optimum value for that particular lens diameter; thus, the image is out of focus. Simulation results track the data very well. The numerical aperture of optimum-size lens B is 0.28, equal to that of lens A. This supports the notion of improving resolution by decreasing magnification through lens dimensional scaling.

The SEM image of Fig. 4(a) is a 7 nm-wide, 41 nm-long trench patterned using Lens B with diameter = 170 nm. The feature width is quite uniform; the linewidth varies by less than 1 nm over its length. The focusing voltage was 96.8 V, with 8 min of dwell time per exposure step. The exposure step size was 4 nm, achieved by tilting the sample stage 0.2° /step. Fig. 4(b) is an SEM image of a 3 nm-diameter hole

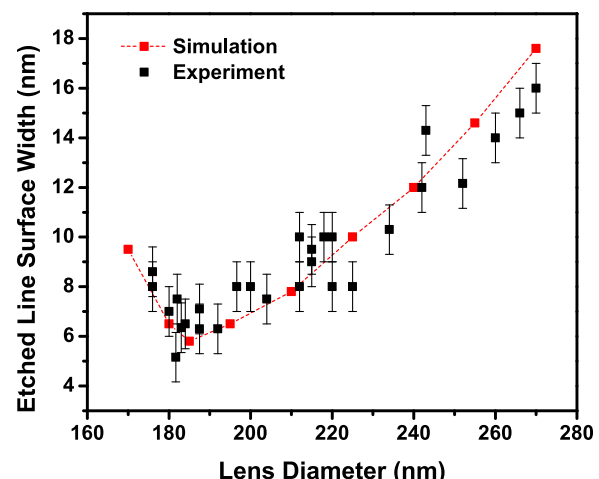


FIG. 3. Comparison between simulation results and experimental data for a constant focusing voltage of 96.8 V and variable lens diameter. Experimental data are shown for two lens arrays fabricated under identical conditions.

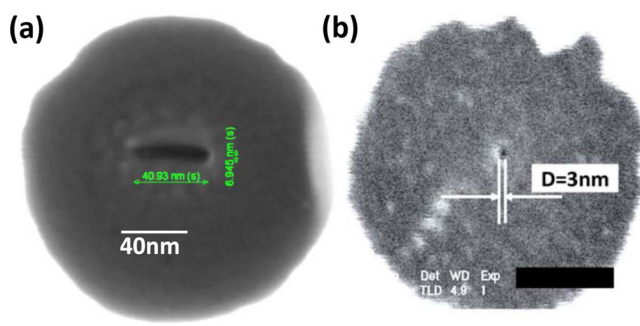


FIG. 4. (a) SEM image of a 7 nm-wide trench written with a 170 nm-diameter lens and a focusing voltage of 96.8 V; (b) SEM image of 3 nm-diameter hole written in a 230 nm-diameter lens with a focusing voltage of 97.7 V. The black scale bar for (b) is 50 nm.

etched in Si at the center of a 230 nm-diameter lens, using a focusing voltage of 97.7 V. This appears to be the smallest feature created using a massively parallel top-down approach.³⁶

In summary, nanofeatures as small as 3 nm were formed by nanopantography, a massively parallel nanopatterning method over large areas. This was achieved by reducing the energy spread and source size of the ion beam, by scaling the lens dimensions, and by optimizing best-focus settings, aided by computer simulation. Such small features, created in a fairly inexpensive tool open possibilities for writing even smaller nanofeatures in a massively parallel fashion.

This work was supported by the National Science Foundation grants CMMI 1030620 and IIP 1343387, and the Department of Energy, Office of Fusion Energy Science. We also acknowledge Dr. L. Chang and Dr. J. Guo of the *UH Nanofabrication Facility* for their help with lens fabrication.

- ¹K. Liu, P. Avouris, J. Buccignano, R. Martel, S. Sun, and J. Michl, *Appl. Phys. Lett.* **80**(5), 865–867 (2002).
- ²K. Trivedi, H. Yuk, H. C. Floresca, M. J. Kim, and W. Hu, *Nano Lett.* **11**(4), 1412–1417 (2011).
- ³X. Wang, Y. Ouyang, X. Li, H. Wang, J. Guo, and H. Dai, *Phys. Rev. Lett.* **100**(20), 206803 (2008).
- ⁴H. Im, K. C. Bantz, N. C. Lindquist, C. L. Haynes, and S.-H. Oh, *Nano Lett.* **10**(6), 2231–2236 (2010).
- ⁵M. R. Gartia, A. Hsiao, A. Pokhriyal, S. Seo, G. Kulsharova, B. T. Cunningham, T. C. Bond, and G. L. Liu, *Adv. Opt. Mater.* **1**(1), 68–76 (2013).
- ⁶K. Schraml, M. Spiegl, M. Kammerlocher, G. Bracher, J. Bartl, T. Campbell, J. J. Finley, and M. Kaniber, *Phys. Rev. B* **90**(3), 035435 (2014).
- ⁷C. Dekker, *Nat. Nanotechnol.* **2**(4), 209–215 (2007).

- ⁸D. Folgea, B. Ledden, D. S. McNabb, and J. Li, *Appl. Phys. Lett.* **91**(5), 053901 (2007).
- ⁹M. Gershov and J. A. Golovchenko, *Nat. Nanotechnol.* **2**(12), 775–779 (2007).
- ¹⁰J. Clarke, H.-C. Wu, L. Jayasinghe, A. Patel, S. Reid, and H. Bayley, *Nat. Nanotechnol.* **4**(4), 265–270 (2009).
- ¹¹P. Xie, Q. Xiong, Y. Fang, Q. Qing, and C. M. Lieber, *Nat. Nanotechnol.* **7**(2), 119–125 (2012).
- ¹²I. Yanagi, T. Oura, T. Haga, M. Ando, J. Yamamoto, T. Mine, T. Ishida, T. Hatano, R. Akahori, T. Yokoi, T. Anazawa, and Y. Goto, *IEEE Int. Electron Devices Meet. (IEDM 13-377)* **2013**, 14.3.1.
- ¹³M. Y. Han, B. Özyilmaz, Y. Zhang, and P. Kim, *Phys. Rev. Lett.* **98**(20), 206805 (2007).
- ¹⁴B. Chitara, L. S. Panchakarla, S. B. Krupanidhi, and C. N. R. Rao, *Adv. Mater.* **23**(45), 5419–5424 (2011).
- ¹⁵K. F. Mak, C. Lee, J. Hone, J. Shan, and T. F. Heinz, *Phys. Rev. Lett.* **105**(13), 136805 (2010).
- ¹⁶G. Eda and S. A. Maier, *ACS Nano* **7**(7), 5660–5665 (2013).
- ¹⁷F. H. L. Koppens, T. Mueller, P. Avouris, A. C. Ferrari, M. S. Vitiello, and M. Polini, *Nat. Nanotechnol.* **9**(10), 780–793 (2014).
- ¹⁸D. Jariwala, V. K. Sangwan, L. J. Lauhon, T. J. Marks, and M. C. Hersam, *ACS Nano* **8**(2), 1102–1120 (2014).
- ¹⁹H. D. Ha, D. J. Han, J. S. Choi, M. Park, and T. S. Seo, *Small* **10**(19), 3858–3862 (2014).
- ²⁰V. R. Manfrinato, L. Zhang, D. Su, H. Duan, R. G. Hobbs, E. A. Stach, and K. K. Berggren, *Nano Lett.* **13**(4), 1555–1558 (2013).
- ²¹R. Ruiz, H. Kang, F. A. Detcheverry, E. Dobisz, D. S. Kercher, T. R. Albrecht, J. J. de Pablo, and P. F. Nealey, *Science* **321**(5891), 936–939 (2008).
- ²²P. Rincon Delgadillo, R. Harukawa, M. Suri, S. Durant, A. Cross, V. R. Nagaswami, D. Van Den Heuvel, R. Gronheid, and P. Nealey, *Proc. SPIE* **8680**, 86800L (2013).
- ²³R. A. Farrell, E. R. Hosler, G. M. Schmid, J. Xu, M. E. Preil, V. Rastogi, N. Mohanty, K. Kumar, M. J. Cicoria, D. R. Hetzer, and A. DeVilliers, *Proc. SPIE* **9051**, 90510Z (2014).
- ²⁴S.-M. Park, X. Liang, B. D. Harteneck, T. E. Pick, N. Hiroshima, Y. Wu, B. A. Helms, and D. L. Olynick, *ACS Nano* **5**(11), 8523–8531 (2011).
- ²⁵J. A. Stroscio and D. M. Eigler, *Science* **254**(5036), 1319–1326 (1991).
- ²⁶D. M. Eigler and E. K. Schweizer, *Nature* **344**(6266), 524–526 (1990).
- ²⁷O. Custance, R. Perez, and S. Morita, *Nat. Nanotechnol.* **4**(12), 803–810 (2009).
- ²⁸L. Xu, S. C. Vemula, M. Jain, S. K. Nam, V. M. Donnelly, D. J. Economou, and P. Ruchhoeft, *Nano Lett.* **5**(12), 2563–2568 (2005).
- ²⁹L. Xu, A. Nasrullah, Z. Chen, M. Jain, P. Ruchhoeft, D. J. Economou, and V. M. Donnelly, *Appl. Phys. Lett.* **92**(1) 013124 (2008).
- ³⁰S. Tian, V. M. Donnelly, and D. J. Economou, *J. Vac. Sci. Technol. B* **33**(3), 030602 (2015).
- ³¹C. M. Osburn and D. W. Ormond, *J. Electrochem. Soc.* **119**(5), 591–597 (1972).
- ³²C. M. Osburn and D. W. Ormond, *J. Electrochem. Soc.* **119**(5), 597–603 (1972).
- ³³P. Solomon, *J. Vac. Sci. Technol.* **14**(5), 1122–1130 (1977).
- ³⁴D. A. Dahl, *Int. J. Mass Spectrom.* **200**(1–3), 3–25 (2000).
- ³⁵S. K. Nam, D. J. Economou, and V. M. Donnelly, *Plasma Sources Sci. Technol.* **16**(1), 90–96 (2007).
- ³⁶R. Garcia, A. W. Knoll, and E. Riedo, *Nat. Nanotechnol.* **9**(8), 577–587 (2014).